Original Article

Journal of Intelligent Material Systems and Structures

Journal of Intelligent Material Systems and Structures
2014, Vol. 25(8) 989–1008

DOI: 10.1177/1045389X13502869
jim.sagepub.com
SAGE

An integrated conceptual design study using span morphing technology

Rafic M Ajaj[1], Michael I Friswell[2], Erick I Saavedra Flores[3], Andy Keane[1], Askin T Isikveren[4], Giuliano Allegri[5] and Sondipon Adhikari[2]

Abstract

A comprehensive conceptual design study is performed to assess the potential benefits of span morphing technology and to determine its feasibility when incorporated on medium altitude long endurance unmanned air vehicles. A representative medium altitude long endurance unmanned air vehicle based on the BAE Systems Herti unmanned air vehicle was selected. Stability and control benefits are investigated by operating the morphing span asymmetrically to replace conventional ailerons. The Tornado vortex lattice method was incorporated for aerodynamic predictions. The sensitivity of rolling moment generated by span morphing for different flight parameters (instantaneous vehicular weight and angle of attack) is studied. The variation of roll rate (steady and transient response) with span morphing (for constant rolling moment) for different rolling strategies (extension and retraction) is investigated. It turns out that the optimum rolling strategy is to extend one side of the wing by 22% while retract the other by 22%. Operational performance benefits are investigated by operating the morphing span symmetrically to reduce drag, increase endurance and reduce take-off and landing distances. Twenty-two per cent symmetric span morphing reduces the total drag by 13%, enhances the endurance capability by 6.5% and reduces the take-off field length and landing distance by 28% and 10%, respectively.

Keywords

Span, morphing, UAV, roll, control, performance

Introduction

Continuous demands to enhance flight performance and control authority have focused the interest of aircraft designers on span morphing. Wings with large spans have good range and fuel efficiency, but lack manoeuvrability and have relatively low cruise speeds. By contrast, aircraft with low aspect ratio wings can fly faster and become more manoeuvrable, but show poor aerodynamic efficiency (McCormik, 1995). A variable span wing can potentially integrate into a single aircraft the advantages of both designs, making this emerging technology especially attractive for military unmanned air vehicles (UAVs). Increasing the wing span increases the aspect ratio and wing area and decreases the spanwise lift distribution for the same lift. Thus, the drag of the wing could be decreased, and consequently, the range or endurance of the vehicle increases. Unfortunately, the wing-root bending moment can increase considerably due to the larger span. Thus, the aerodynamic, structural, aeroelastic and control characteristics of the vehicle should be investigated in the design of variable span morphing wings. Most span morphing concepts are based on a telescopic mechanism, following the ideas of Ivan Makhonine, a Russian expatriate, where the wing outer panel telescoped inside the inner panel to enable span and wing area changes. The MAK-10 was the first design with a telescopic wing and it first flew in 1931. The mechanism was powered pneumatically and enabled span increases up to 62% (from 13 to 21 m) and area increases up to 57% (from 21 to 33 m^2) (Weisshaar, 2006). Blondeau and Pines (2007) designed and fabricated a three-segmented telescopic wing for a UAV. Hollow fibreglass shells were used to preserve the spanwise aerofoil geometry and ensure compact storage and deployment

[1]Aeronautics and Astronautics, University of Southampton, Southampton, UK.
[2]College of Engineering, Swansea University, Swansea, UK
[3]Departamento de Ingeniería en Obras Civiles, Universidad de Santiago de Chile, Santiago, Chile
[4]Bauhaus Luftfahrt e.V., Munich, Germany
[5]Department of Aerospace Engineering, University of Bristol, Bristol, UK

Corresponding author:
Rafic M Ajaj, Aeronautics and Astronautics, University of Southampton, Southampton, UK, SO171BJ.
Email: r.ajaj@southampton.ac.uk.

of the telescopic wing. To reduce the weight, they replaced the wing spars with inflatable actuators that could support the aerodynamic loads on the wing (in excess of 73 kg/m^2). Their telescopic spar design consisted of three concentric circular aluminium tubes of decreasing diameter and increasing length, connected by ceramic linear bearings, and deployed and retracted using input pressures of 345–483 kPa (50–70 lbf/in^2). The wing could undergo a 114% change in the aspect ratio while supporting aerodynamic loads.

Blondeau et al. (2003) adopted two identical telescopic spars instead of one, mechanically coupled by the ribs, to prevent wing twist and fluttering. The new prototype could undergo a 230% change in aspect ratio, and seam heights were reduced giving less parasitic drag. In its fully deployed condition the telescopic wing could achieve lift-to-drag ratios as high as 16, which was similar to its solid foam-core wing counterpart. The most dramatic morphing wing involving span change that has been realised as a wind tunnel prototype is the Agile Hunter by Lockheed Martin (Bye and McClure, 2007; Ivanco et al., 2007; Love et al., 2007). Funded by defense advanced research projects agency (DARPA) within the morphing aircraft structures (MAS) program, the prototype was based on a military UAV capable of folding the inner sections of the wing near the fuselage, to reduce the surface area and drag during transonic flight at low altitude (also called a Z-wing). The major challenge was the realisation of suitable hinges that connect the two wing portions; the hinges have to sustain the aerodynamic loads but offer a smooth, continuous aerodynamic surface. Several materials were considered, including silicone-based and shape memory polymer skins. Wind tunnel tests at Mach 0.6 showed a morphing capability from 0° to 130° over 65 s with a controllable, reliable and precise actuation.

Asymmetrical span morphing can be used for roll control. Ajaj et al. (2012) investigated the use of asymmetric span morphing to replace conventional ailerons and provide roll control for a medium altitude long endurance (MALE) UAV. In addition, they optimised the rolling strategy to minimise drag for a steady roll manoeuvre. Seigler et al. (2004) investigated asymmetrical span extension for increased manoeuvrability of bank-to-turn cruise missiles. By formulating a full nonlinear model of the missile, due to the shift of the missile centre of mass and the dependence of the rolling moment on the angle of attack (AOA), they showed that the control authority can be significantly larger when compared to conventional tail surface control. Improved manoeuvrability, however, is highly dependent on the AOA, linear actuation speed and extension length. Moreover, as the mass of the extending wings becomes large relative to the missile body, the rigid body dynamics can become increasingly complex and a non-linear control law was formulated to control the roll, AOA and sideslip angle dynamics in accordance with bank-to-turn guidance. The control method proved to be adept in tracking commanded inputs while effectively eliminating sideslip. A more extensive review on span morphing technology (applications and concepts) for both fixed-wing and rotary-wing aircraft is given in Barbarino et al. (2011).

In contrast to feasibility studies in the literature, this article performs a comprehensive conceptual design study to determine the potential benefits (control and performance) of span morphing and assess its practicality on a MALE UAV from a conceptual design point of view. The main target of the article is to show that even if morphing technologies are heavier and more complicated than conventional technologies, their multiple functionalities and capabilities keep them potential candidates in terms of overall benefits. Stability and control benefits are investigated by operating the morphing span asymmetrically to replace conventional ailerons. For span morphing to be a successful roll device it must provide the required rolling moment and rolling rate throughout the entire mission profile of the UAV. The variation of rolling rate with different rolling strategies is investigated and compared to conventional ailerons by modifying the roll equation of motion. Operational performance benefits are investigated by operating the morphing span symmetrically to reduce drag, increase endurance and reduce take-off and landing distances (LDs). The sensitivity of the performance benefits to a range of weight penalties associated with span morphing is also considered. It should be highlighted that a UAV with a simple mission profile is used in this study to assess the potential benefits of the span morphing technology. However, the ultimate objective with morphing technology is to be able to perform a range of missions (strike, cruise and loiter) with different levels of agility and manoeuvrability. Those missions can have different speeds and altitudes and therefore a non-morphing long wing with ailerons cannot provide the flexibility and effectiveness that can be achieved with span morphing. The multi-mission capability is the main driver for this study; however, this article focuses mainly on the loiter mission and the benefits of span morphing for the other multi-missions will be considered in future work.

Aerodynamics

The Tornado vortex lattice method (VLM) was used for aerodynamic predictions. Tornado is a linear aerodynamics code, and thus it discounts wing thickness and viscous effects (Melin, 2000). These limitations imply that Tornado can only be used for angles of attack up to 8°–10° for slender wings. Linear aerodynamic theory is still nevertheless very useful as most aircraft typically operate within the linear region (operating lift coefficients at reference speeds) in cruise/endurance, as well as both take-off and landing phases. These are the flight stages in which most of this

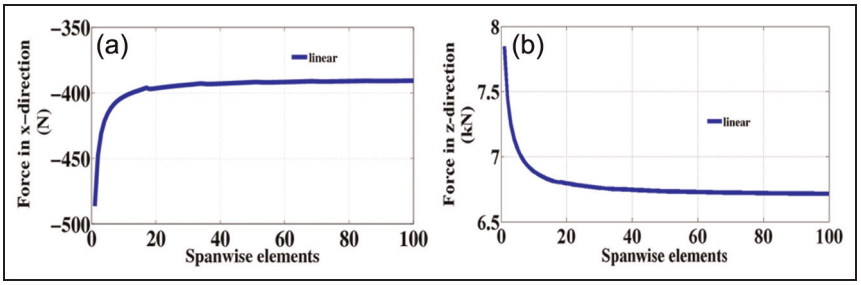

Figure 1. Variation of aerodynamic forces with spanwise elements: (a) force in the *x*-direction and (b) force in the *z*-direction.

research and analysis has been undertaken. In Tornado, usually one half of the wing is built and then mirrored with respect to the centreline of the aircraft to generate the entire wing. In order to investigate roll control using span morphing, each half of the wing is built separately to allow the asymmetric change in span. Typically the wing is defined from the root to the tip in Tornado for the symmetric case. However for the asymmetric case, one half of the wing is defined from root to tip and the other half is defined from tip to root. As the wing semi-span starts to increase the size of the spanwise elements start to increase resulting in coarser aerodynamic mesh. A convergence study was performed to determine the size of the aerodynamic mesh required to generate accurate and robust results. The number of elements in the chordwise direction was fixed to five elements and only the spanwise density was changed. The variation with the overall forces in the *x*- and *z*-directions (Figure 3) with the number of spanwise elements is shown in Figure 1.

As the number of elements increases, the accuracy of the prediction improves but the computation time increases greatly. Twenty elements are sufficient to provide robust prediction with a relative error of 0.05%. A linear distribution for the spanwise and chordwise panels was adopted.

Asymmetric span morphing

A MALE UAV similar to the BAE Systems Herti UAV (Austin, 2010) (shown in Figure 2) was selected for this study. The UAV is modelled in Tornado VLM as shown in Figure 3 and has a maximum lift-to-drag ratio of about 20 and a maximum endurance capability of about 18 h. Figure 3 also shows the position of the mean aerodynamic chord (MAC). A representative flight profile, as shown in Figure 4, was assumed in this analysis. The UAV takes off with a weight of 800 kg and it cruises and loiters for about 18 h with a speed of 50 m/s (M0.16) at 6100 m (20,000 ft) and then it descends and lands. The weight fractions, namely, instantaneous gross weight normalised by the gross weight at the start of the flight segment (Raymer, 2006), of the vehicle are listed in Table 1. The design weights of the vehicle are given in Table 2.

Figure 2. The BAE Systems Herti UAV (Austin, 2010).
UAV: unmanned air vehicle.

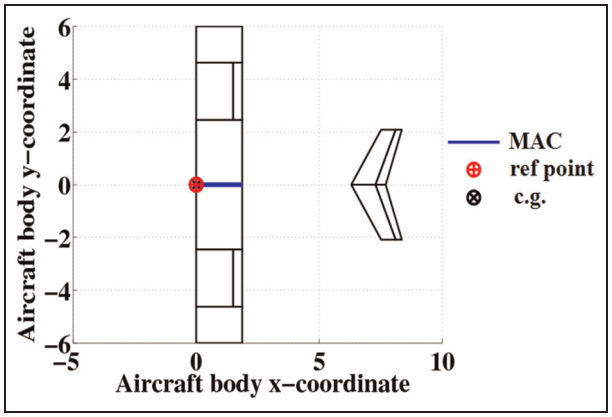

Figure 3. The MALE UAV in Tornado.
MALE: medium altitude long endurance; UAV: unmanned air vehicle; MAC: mean aerodynamic chord.

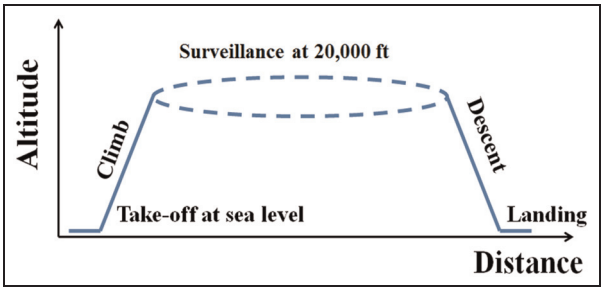

Figure 4. Mission profile of the UAV.
UAV: unmanned air vehicle.

Table 1. Weight fractions of the UAV.

Mission segments	Weight fraction (W_i/W_{i-1})
Take-off	0.9875
Endurance	0.8354
Descent	0.9875

UAV: unmanned air vehicle.

Table 2. UAV design weights.

Design weights	Values (kg)
MTOW	800
BOW (estimated)	500
Fuel weight (estimated)	150
Wing weight (estimated)	120
Payload	150

UAV: unmanned air vehicle; MTOW: maximum take-off weight; BOW: basic operating weight.

Four representative points on the flight envelope are considered in this article. These correspond to take-off, start of loiter, end of loiter and landing. The instantaneous flight conditions and vehicular weight at those points are given in Table 3. Furthermore, Table 3 contains the maximum allowable aileron angle at each of these flight points. These values are assumed based on similar UAVs due to the lack of data. Similar UAVs have a maximum aileron angle of 15° in both upwards and downwards, and during high-speed phases about 70% of the maximum angle is required.

At each of the flight points listed in Table 3, the maximum rolling moment generated by the ailerons and the adverse yawing moment associated with it are computed. The ailerons are assumed to deflect asymmetrically with the same angle but opposite directions. For span morphing, the span of one side of the wing is increased gradually until it reaches a point where the rolling moment from span morphing is equal to the rolling moment generated by the ailerons. It should be noted that in all the calculations performed by Tornado VLM, the total lift (before or after extension) is always equal to the instantaneous weight of the vehicle to ensure that the altitude remains constant as the vehicle starts to roll. This is achieved by continuously adjusting the AOA as the wing span increase to maintain steady flight. The required span extensions at take-off, start of endurance, end of endurance and landing were computed and are listed in Table 4. Note that the lateral shift of the centre of gravity associated with asymmetric span morphing is neglected in this analysis.

It turns out that the maximum semi-span extension required is at the end of loiter flight point, where about 43% extension in the wing semi-span is required. Figure 5 shows the variation of the rolling moment coefficient (C_l) and the yawing moment coefficient (C_n) with semi-span extension and aileron angle at the end of loiter (where maximum extension is required) obtained from Tornado VLM.

It can be seen that the variation of the rolling moment coefficient and the yawing moment coefficient is linear with the aileron angle. This is because Tornado VLM is a linear aerodynamic code. On the contrary, the rolling moment coefficient and the yawing moment coefficient variations with span extension are almost parabolic very close to being linear. The coefficient of determination (R^2) is 0.996 when linear fitting is used. The rates of change of the rolling and yawing moment coefficients with span extension tend to increase slightly as wing semi-span is increased.

Sensitivity to vehicular weight

Table 4 shows that the semi-span extension required for roll control varies between the start of loiter and

Table 3. Flight conditions at the selected flight points.

Flight point	Weight (kg)	Speed (m/s)	Altitude (m)	Angle of attack (°)	Aileron angle (°)
Take-off	800	25	0	10.9	15
Start of loiter	790	50	6100	5.0	10
End of loiter	660	50	6100	4.2	10
Landing	650	20	0	13.9	15

Table 4. Estimated moments generated by semi-span extension.

Flight point	Semi-span extension (%)	Rolling moment (N m)	Yawing moment from span (N m)	Yawing moment from aileron (N m)
Take-off	25	5323	791	1100
Start of loiter	36	7708	548	1329
End of loiter	43	7730	454	1297
Landing	19	3326	642	748

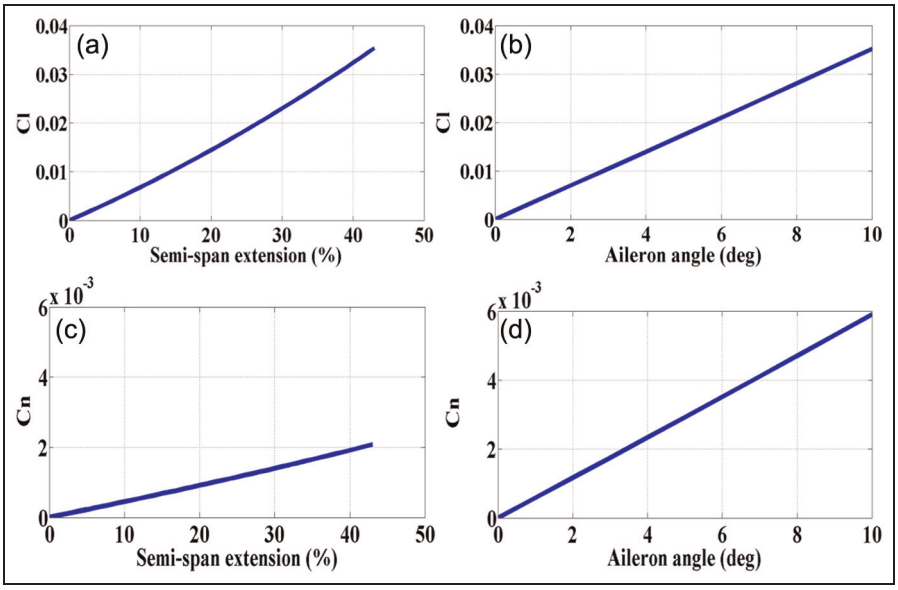

Figure 5. Variation of rolling and yawing moment coefficients at end of loiter: (a) rolling moment coefficient with span extension, (b) rolling moment coefficient with aileron angle, (c) yawing moment coefficient with span extension and (d) yawing moment coefficient with aileron angle.

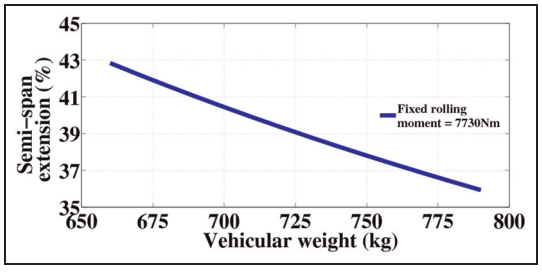

Figure 6. Variation of semi-span extension with vehicular weight at 6100 m and 50 m/s.

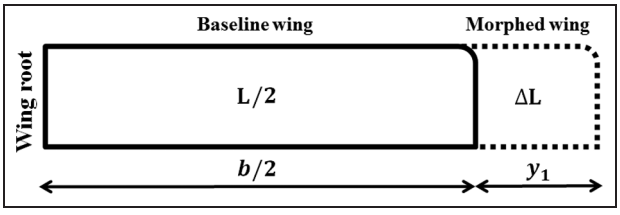

Figure 7. Sketch of the span morphing wing.

the end of loiter by 7% even though the desired rolling moment is almost the same. Therefore, it is of great interest to understand the variation of the span extension required as the UAV burns fuel while loitering at a constant altitude and speed.

Figure 6 above shows that as the vehicle burns fuel at constant altitude and speed, the semi-span extension required to generate 7730 Nm increases from 36% to 43%. The sensitivity of the span morphing to vehicular weight infers that it is also sensitive to the instantaneous AOA because weight and AOA are directly related at steady level flight. In other words, the magnitude of rolling moment achieved by span extension depends on the magnitude of the lift force generated by the wing or lifting surface prior to changing the span. To understand the sensitivity of required semi-span extension to the instantaneous vehicular weight, a simplified expression of rolling moment is established. After the semi-span of the wing extends a distance y_1, as shown in Figure 7, the total lift at the start of roll must always balance the weight (to avoid gaining or losing altitude), and hence the total lift, L + ΔL, becomes

$$\mathrm{L} + \Delta\mathrm{L} = qC_L(S + \Delta S) = Wg \tag{1}$$

where L is the instantaneous lift generated by the original wing before span extension, ΔL is the change in lift due to span extension, q is the dynamic pressure, C_L is the lift coefficient, S is the original wing area, ΔS is the change in wing area due to span morphing, W is the vehicular weight in kilograms and g is the gravitational acceleration. Before span extension the lift, L, was equal weight, but after span extension the AOA is reduced so this lift is reduced and when summed with the lift due to the extension, ΔL, it becomes equal to the weight. For a rectangular wing, the area and change in area become

$$S = bc \tag{2}$$

and

$$\Delta S = cy_1 \tag{3}$$

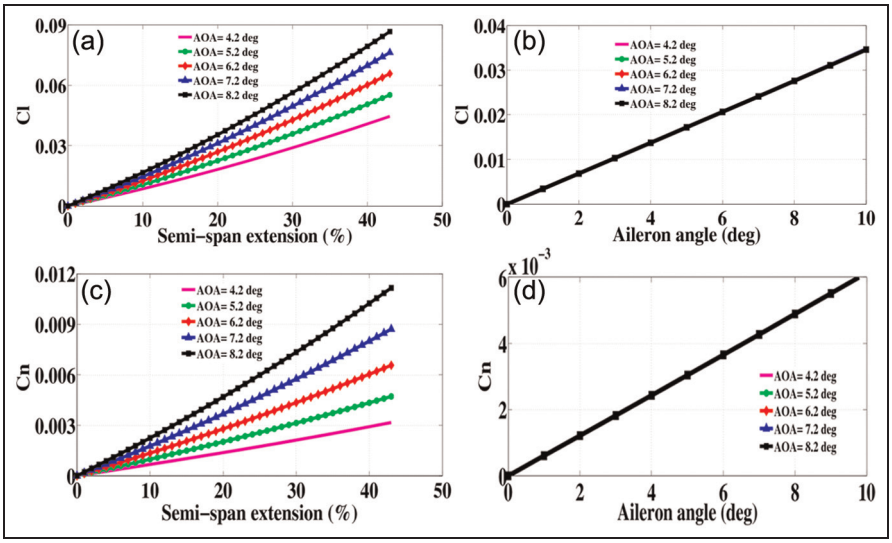

Figure 8. Variation of rolling and yawing moment coefficients from span morphing and aileron angle with the AOA at M0.16, 20,000 ft: (a) variation rolling moment coefficient with span extension, (b) variation rolling moment coefficient with aileron angle, (c) variation yawing moment coefficient with span extension and (d) variation yawing moment coefficient with aileron angle.
AOA: angle of attack.

where b is the original wing span and c is the wing chord. The total lift coefficient can be expressed as

$$C_L = \frac{Wg}{qc(b + y_1)} \tag{4}$$

The rolling moment, L_s, generated by semi-span extension is approximately

$$L_s \approx \Delta L\left(\frac{b}{2} + \frac{y_1}{2}\right) \approx qcy_1 C_L\left(\frac{b}{2} + \frac{y_1}{2}\right) \tag{5}$$

Equation (5) assumes ΔL acts in the midpoint of the extension, and hence it has a total moment arm of $((b/2) + (y_1/2))$. By substituting expression for C_L given into equation (4), the rolling moment becomes

$$L_s \approx \frac{Wg}{2} y_1 \approx \frac{L}{2} y_1 \tag{6}$$

Equation (6) shows that for a desired rolling moment, the required semi-span extension is inversely proportional to the instantaneous vehicular weight. Furthermore, equation (6) infers that for a given semi-span extension, the rolling moment generated depends on the wing lift prior to the extension and during steady flight the weight is almost equal to the wing lift (neglecting other contributions of lift). This explains why for a given rolling moment the maximum semi-span extension required is at the end of loiter and the minimum span extension required is at the start of loiter.

Sensitivity to AOA

It was of interest to see how the variation of AOA at the end of loiter flight point is varied and the variation in span morphing is computed and compared to conventional ailerons. Figure 7 shows that the rolling moment and yawing moment coefficients for a given span extension increase significantly as the AOA is increased. For instance, at 10% extension in the wing semi-span, the rolling moment is 0.007 at AOA of 3.3° and 0.0115 at AOA of 5.9°. In contrast, Figure 8 shows that the rolling moment and yawing coefficients generated by the ailerons are independent of AOA for any given aileron angle. This because the rolling and adverse yawing moments generated by the ailerons depend only on the aileron angle, aileron dimensions, aileron spanwise position and the dynamic pressure but not the AOA (according to Tornado VLM assumptions).

The above figure shows that it is very efficient to pitch and extend the wing span simultaneously to maximise the rolling authority of the vehicle. Such a manoeuvre (coupling pitch and roll) can be of great interest for military UAVs that require large rolling authority (moment and rate), but this depends on the type of manoeuvre to be performed. These results raise important issues about morphing technologies. These issues are given below.

- Morphing technologies should not be operated in the same way as conventional technologies.
- If the operation of vehicles with morphing technologies is conducted in the same way as conventional technologies, this limits the benefits of morphing and reduces its effectiveness in competing with very mature conventional technology.
- The benefits of morphing technologies can be significantly enhanced by exploiting existing

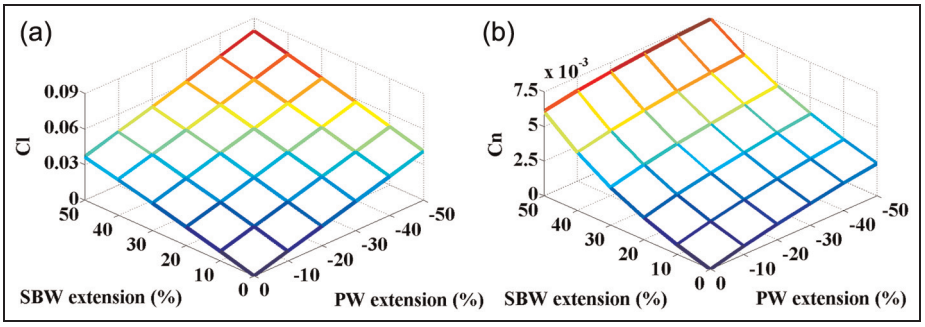

Figure 9. Variation of rolling and yawing moment coefficients with span morphing at M0.16, 20,000 ft: (a) variation of rolling moment coefficient and (b) variation of yawing moment coefficient.
SBW: starboard wing; PW: port wing.

Table 5. Optimising the rolling manoeuvre.

Objective function	Minimise (C_D)
Variables	y_1 change in starboard wing span (m) y_2 change in port wing span (m)
Constraints	$0 \leq y_1 \leq 2.6$ m $-2.6 \leq y_2 \leq 0$ m $L_s = 7730$ Nm

coupling effects (in this case: pitch and roll), which have been disregarded throughout the design of conventional structures to simplify the analysis and the design of the control law.

Optimum rolling strategies

In the above section, the roll manoeuvre was achieved by extending the span of one side of the wing while keeping the span on the other side fixed. Obviously, from a structural perspective, this is not the best strategy to achieve roll control because it increases the root bending moment significantly and it requires larger local strains if active complaint structures are to be employed. Thus, it is more practical to investigate morphing of both sides of the wing (extension and retraction independent on each side). The variations of the rolling moment and yawing moment coefficients with span extension of the starboard wing (SBW) and the retraction port wing (PW) are shown in Figure 9. Note that the AOA for each point in Figure 9 is adjusted to maintain steady flight after morphing prior to rolling.

Figure 9(a) shows that the variation of C_l with span extension has some degree of curvature (due to the parabolic effect shown in Figure 5(a) but as a first-order approximation it is approximately linear. It can be noticed that for a required C_l, different number of span morphing combinations (SBW and PW) are possible. It should be noted that the coefficients in Figure 9 are normalised by the original wing area and original wing span, that is, before morphing occurs, in order to allow for direct comparison of the results.

To obtain the optimum combination of span morphing for a given objective and conflicting constraints, the genetic algorithm (GA) optimiser was used. The GA is a stochastic global search and optimisation method. The GA mimics the metaphor of natural evolution by applying the principle of the survival of the fittest to produce successively better approximations to a solution. The 'Matlab GA Toolbox', developed by Chipperfield and Fleming (1995), was incorporated in this analysis. A fitness value is assigned to every individual of the initial population through an objective function that assesses the performance of the individual in the problem domain. Then, individuals are selected based on their fitness index and crossover between them is performed to generate new offspring. Finally, mutation of the new offspring is performed to ensure that the probability of searching any subspace of the problem is never zero. These processes iterate until the optimum solution is achieved depending on the convergence criteria of the problem. The selection of the best combination depends on the objective function and on the constraints. A GA run of 25 generations and 25 individuals is performed. In this section, the objective is to minimise the total drag coefficient for various constraints. The optimisation problem is summarised in Table 5.

In Table 5 C_D is the total drag coefficient of the UAV and L_s is the rolling moment generating by span morphing. In order to compute the drag coefficient associated with pure roll, the rudder is deflected to counteract the adverse yawing moment generated by asymmetric span morphing. This contributes mainly to the induced drag coefficient. The drag was selected as an objective function as it is directly related to the excess power that feeds indirectly into the agility and manoeuvrability.

In the above section, approximately 43% semi-span extension was required to meet the roll control

Table 6. Optimum rolling strategies.

Rolling strategy	$C_D(\times 10^{-4})$	Rudder angle (°)	BM_r (kN m)	Constraint(s)	y_1 (m)	y_2 (m)
Ailerons	210	1.5	11.3	–	–	–
SBW 43% PW 0%	154	0.6	15.7	–	2.6	–
SBW 22% PW −22%	172	0.9	13.9	$y_1 + y_2 \geq 0\%$ $BM_r \leq 14.7$ kN m	1.32	−1.32
SBW 4% PW −43%	201	1.4	12.2	$BM_r \leq 12.4$ kN m	0.24	−2.6

SBW: starboard wing; PW: port wing.

requirements of the vehicle. The associated overall drag coefficient is 0.0154 and the root bending moment, BM_r, is 15.70 kN m. The drag coefficient associated with the ailerons is 0.0210 and the root bending moment is 11.30 kN m. Two rolling cases are investigated in this section. The first case is when the root bending moment generated by span morphing must not be greater than that produced by the ailerons by more than 30% and the area of the wing must not be smaller than the original wing area. In contrast, in the second case the area constraint is removed and a more stringent root bending moment constraint is added where the root bending moment from span morphing must not be greater than that of the ailerons by more than 10% to avoid redesigning the wing root section. Table 6 summarises the results for each rolling strategy. It should be noted that in both cases, as the wing area is altered due to span morphing, the AOA is altered to ensure the lift balances the weight and to avoid losing or gaining altitude at the start of roll. All the analyses performed were at the end of loiter flight point where the maximum semi-span extension is needed. It should be noted that in all the rolling strategies the rolling moment generated is equal to 7730 Nm which implies that the strategies are compared according to their aerodynamic efficiency (minimum drag) for a given level of agility. This is necessary to ensure consistency in the comparison and to justify the selection of drag to be the objective function.

The parameter BM_r is the root bending moment (maximum of moments on both sides). Table 6 shows that from an aerodynamic point of view it is superior to achieve the roll manoeuvre by extending one side of the wing by 43% while keeping the other side fixed to maximise the overall span of the wing. Also, it should be noted that the rudder angle required to counteract the adverse yawing moment is minimum for morphing only one side of the wing. However, from a structural point of view, this results in a very large root bending moment about 40% higher than that produced by the ailerons. To roll at the same altitude, it is optimum to morph both sides of the wing by the same amount but opposite directions. This increases the drag coefficient slightly by 11.7% but reduces the root bending moment by about 17% in comparison to morphing one side only. On the contrary, when a stringent root bending moment constraint is added and the span constraint is removed, the drag coefficient increases by 30% and the root bending moment is reduced by about 30% in comparison to morphing one side only. The different morphing strategies are shown in Figure 10. Table 6 illustrates that all the morphing strategies are superior to conventional ailerons in generating lower overall drag allowing the vehicle to be more manoeuvrable and agile.

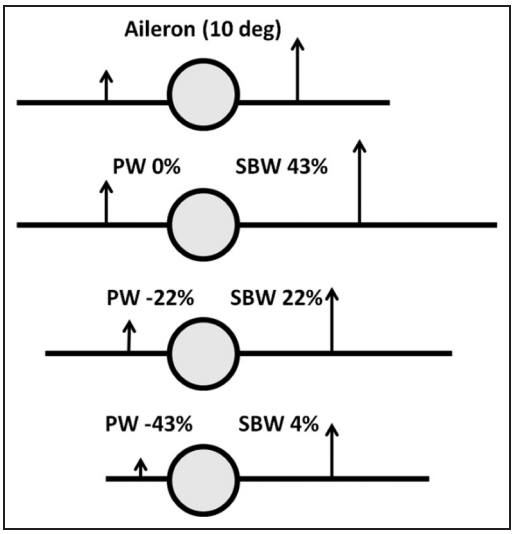

Figure 10. Schematic of the different rolling strategies. SBW: starboard wing; PW: port wing.

Roll rate

Other than matching the rolling moment produced by the ailerons, the speed of response or the roll rate of the vehicle to span morphing must be in the same order of magnitude as the roll rate with aileron deflection. For a pure roll manoeuvre, the first-order differential equation (ODE) can be expressed as (Nelson, 1989)

$$L = I_{xx}\dot{p} + p\dot{I}_{xx} \tag{7}$$

where I_{xx} is the mass moment of inertia of the vehicle around the x-axis and p is the roll rate. For an aileron

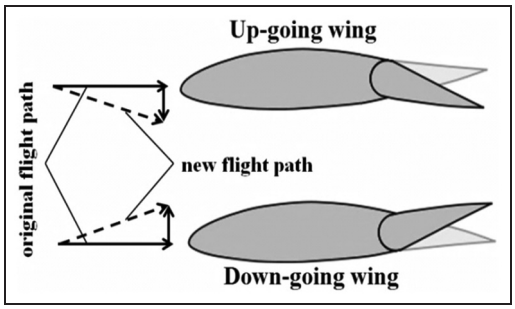

Figure 11. Roll damping phenomenon.

the change in the inertia of the vehicle can be neglected, and hence the rolling equation becomes

$$L = I_{xx_a}\dot{p} = \frac{\partial L}{\partial \delta}\delta + \frac{\partial L}{\partial p}p \tag{8}$$

where δ is the aileron angle. The first term $((\partial L/\partial\delta)\delta)$ in equation (8) represents the rolling moment generated by the ailerons while the second term $((\partial L/\partial p)p)$ represents an aerodynamic damping moment. The rolling motion induces an AOA increase on the down-going wing, and an AOA decrease on the up-going wing which creates an opposing moment known as the roll damping moment. This can be visualised in Figure 11.

The rolling moment generated by the aileron can be expressed as

$$\frac{\partial L}{\partial \delta}\delta = qSb\frac{\partial C_l}{\partial \delta}\delta \tag{9}$$

The roll damping moment can be expressed as

$$\frac{\partial L}{\partial p}p = qSb\frac{\partial C_l}{\partial p} = \frac{\rho U c b^3}{4}C_{l_{pa}}p \tag{10}$$

where ρ is the air density, U is the true airspeed and $C_{l_{pa}}$ is the rolling moment damping coefficient for the wing with ailerons. According to Anderson (1991), the rolling moment damping coefficient for a rectangular wing may be approximated by

$$C_{l_{pa}} = \frac{\pi b}{3(b+2c)} \tag{11}$$

Equation (8) is rearranged to give the following first ODE

$$I_{xx_a}\dot{p} - \frac{\rho U c b^3}{4}C_{l_{pa}}p = qcb^2\frac{\partial C_l}{\partial \delta}\delta \tag{12}$$

where (I_{xx_a}) is the mass moment of inertia of the vehicle with ailerons, assuming a uniform mass distribution of the wing and neglecting the contribution of the fuselage and empennage, it can be expressed as

$$I_{xx_a} \approx \frac{m_w b^2}{12} \tag{13}$$

where m_w is the mass of the wing and estimated to be 120 kg using semi-empirical correlation from Roskam (2003) for general aviation aircraft. On the contrary, the mass moment of inertia (I_{xx_s}) of the vehicle with variable span wing can be expressed as

$$\begin{aligned} I_{xx_s} &\approx \frac{m_w b^2}{12} + \frac{m_w}{6}\left(y_1^2 + y_2^2 + by_1 + by_2\right) \\ &= I_{xx_a} + \frac{m_w}{6}\left(y_1^2 + y_2^2 + by_1 + by_2\right) \end{aligned} \tag{14}$$

It should be noted that in equations (13) and (14) the contribution of the fuselage and empennage to the mass moment of inertia is neglected. The rate of change of the wing inertia can be expressed as

$$\dot{I}_{xx_s} = \frac{m_w}{6}(2y_1\dot{y}_1 + 2y_1\dot{y}_2 + b\dot{y}_1 + b\dot{y}_2) \tag{15}$$

The rolling moment equation for span morphing becomes

$$L = I_{xx_s}\dot{p} + p\dot{I}_{xx_s} = \frac{\partial L}{\partial y_1}y_1 + \frac{\partial L}{\partial y_2}y_2 + \frac{\partial L}{\partial p}p \tag{16}$$

By rearranging the above equation, the following first ODE is obtained

$$I_{xx_s}\dot{p} - \left(\frac{\partial L}{\partial p} - \dot{I}_{xx_s}\right)p = \frac{\partial L}{\partial y_1}y_1 + \frac{\partial L}{\partial y_2}y_2 \tag{17}$$

where

$$\frac{\partial L}{\partial p} = \frac{\rho U c (b + y_1 + y_2)^3}{4}C_{l_{ps}} \tag{18}$$

and

$$C_{l_{ps}} = \frac{\pi(b + y_1 + y_2)}{3(b + y_1 + y_2 + 2c)} \tag{19}$$

The ODEs in equations (12) and (17) can be solved analytically assuming a step input, that is, for the final values of δ, y_1 and y_2 or numerically if the variation of δ, y_1 and y_2 with actuation time are considered.

For a step input, the solutions of the ODEs becomes

- For aileron

$$p(t) = -\frac{2U}{b}\frac{C_{l_\delta}}{C_{l_{pa}}}\delta\left(e^{-t/\tau_a} - 1\right) \tag{20}$$

where, τ_a can be expressed as

$$\tau_a = -\frac{4I_{xx_a}}{\rho U c b^3 C_{l_{pa}}} \tag{21}$$

- For span morphing

Table 7. Time variation of control displacements.

Rolling strategy	Variation (actuation time = 0.5 s)	Variation (actuation time = 1 s)
Aileron	$\delta(t) = 20t$	$\delta(t) = 10t$
SBW 43% PW 0%	$y_1(t) = 5.16t$	$y_1(t) = 2.58t$
	$y_2(t) = 0$	$y_2(t) = 0$
SBW 22% PW −22%	$y_1(t) = 2.64t$	$y_1(t) = 1.32t$
	$y_2(t) = -2.64t$	$y_2(t) = -1.32t$
SBW 4% PW −43%	$y_1(t) = 0.48t$	$y_1(t) = 0.24t$
	$y_2(t) = -5.16t$	$y_2(t) = -2.58t$

SBW: starboard wing; PW: port wing.

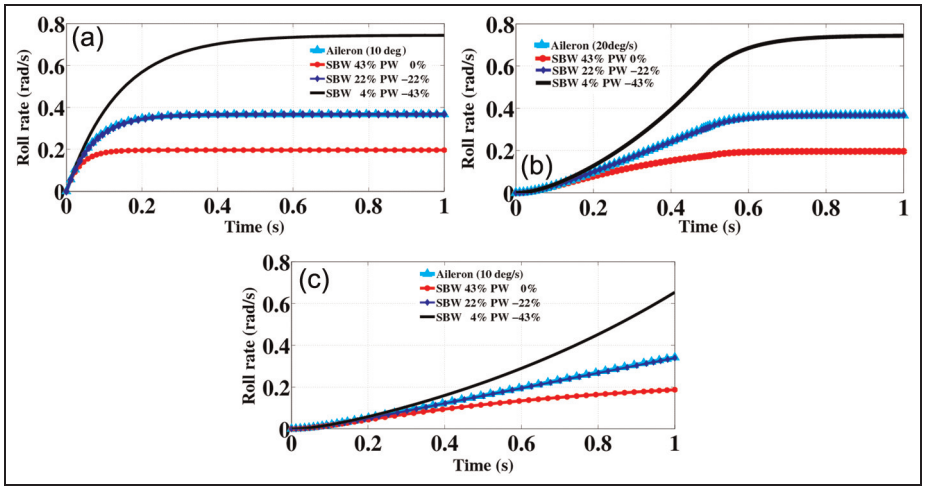

Figure 12. Roll rate for different rolling strategies at M0.16, 20,000 ft: (a) step input, (b) actuation time of 0.5 s and (c) actuation time of 1.0 s.
SBW: starboard wing; PW: port wing.

$$p(t) = -\frac{\frac{\partial L}{\partial y_1} y_1 + \frac{\partial L}{\partial y_2} y_2}{\left(\frac{\partial L}{\partial p}\right)} \left(e^{-t/\tau_s} - 1\right) \tag{22}$$

where the time constant, τ_s, can be expressed as

$$\tau_s = -\frac{4I_{xx_s}}{\rho U c (b + y_1 + y_2)^3 C_{l_{p_s}}} \tag{23}$$

It should be noted that rate of change of inertia ($\dot{I}_{xx_s}$) is zero for the step input case. In this study the terms ($\partial L/\partial y_1$) and ($\partial L/\partial y_2$) are estimated using Tornado VLM. But as a first-order approximation using a first-order, two-variable polynomial fitting, ($\partial L/\partial y_1$) is approximately 0.0007 and ($\partial L/\partial y_2$) is approximately −0.0018.

On the contrary, when the variations of wing span and aileron angle with actuation are considered, explicit solutions for the above ODEs are not possible, and they must be solved numerically. The time variations listed in Table 7 are assumed. Those variations correspond to uniform rates of actuation (constant speed). The response in terms of roll rate is estimated for the step input case and for the dynamic case as shown in Figure 12(a) to (c).

The roll rate values for the step input case and the dynamic cases (0.5 and 1.0 s) are summarised in Table 8. It should be noted that in reality the step input case is not practical and representative for span morphing due to the relatively high weight which requires very large actuation force/power to actuate it very fast. Nevertheless, the results from the step input are crucial to clearly illustrate the difference between the ideal case (step input) and the actual case (time variation).

Based on the above analysis, it can be concluded that 22% extension in SBW and −22% retraction in the PW is the optimum rolling strategy when considering different design aspects. From a structural point of view, it is more feasible than ±43% extension or retraction due to lower root bending moments. In addition, from an aerodynamic point of view it is superior to conventional ailerons producing 18% lower total drag as a bi-product. Finally, in terms of roll rate, it is capable of

Table 8. Roll rate for different rolling strategies.

Rolling strategy	Step input		Dynamic	
	Rate (rad/s)	Time constant (τ) (s)	Rate at 0.5 s (rad/s)	Rate at 1.0 s (rad/s)
Ailerons	0.3671	0.0685	0.3670	0.3414
SBW 43% PW 0%	0.1965	0.0366	0.1965	0.1870
SBW 22% PW −22%	0.3673	0.0718	0.3670	0.3392
SBW 4% PW −43%	0.74430	0.1388	0.7430	0.6540

SBW: starboard wing; PW: port wing.

generating almost the rolling rate as conventional ailerons with a slightly higher time constant.

Symmetric span morphing

In the previous section, the feasibility of span morphing for roll control was discussed. The main focus while designing morphing aircraft is to maximise the functionality of a certain technology or system to enhance commonality, reduce complexity and improve the operation of the vehicle. Therefore (to maximise synergy and functionality), the span morphing system that operated asymmetrically for roll control can be operated symmetrically to enhance flight performance during loiter, increase endurance and improve the operational performance during low-speed transitional flight phases.

Wing drag

The total drag of the wing consists of two major components, parasitic drag (zero lift drag) and vortex-induced drag. The total drag of the wing (D_w) becomes

$$D_w = D_{o_w} + D_i \tag{24}$$

where D_{o_w} is the parasitic drag of the wing and D_i is the vortex-induced drag. It should be noted that for this section, the form drag is neglected, and hence the parasitic drag is only the skin friction drag. The induced drag can be expressed as

$$D_i = qSC_{D_i} = qbc\frac{C_L^2}{\pi eAR} \tag{25}$$

where e is the Oswald efficiency, AR is the wing aspect ratio and C_L is the lift coefficient. For steady level flight, the lift coefficient (without the morphing term as in equation (4)) can be expressed as

$$C_L = \frac{Wg}{qS} = \frac{Wg}{qbc} \tag{26}$$

Therefore, the induced drag can be expressed as

$$D_i = \frac{g^2}{\pi qe}\left(\frac{W}{b}\right)^2 \tag{27}$$

The parasitic drag can be expressed as

$$D_{o_w} = qSC_{Do_w} = qcb\frac{C_{f_e}S_{wet}}{S} \tag{28}$$

where C_{f_e} is the equivalent skin friction coefficient of the wing, and from Tornado VLM, it can be approximated as 0.00323 and (S_{wet}/S) is the ratio of the wing wetted area to the wing reference area and it can be assumed fixed and equal to 2.05 (Raymer, 2006). Thus

$$D_w = qC_{f_e}\left(\frac{S_{wet}}{S}\right)cb + \frac{g^2}{\pi qe}\left(\frac{W}{b}\right)^2 \tag{29}$$

The variation of e with wing span or aspect ratio for a straight wing can be approximated as (Raymer, 2006; Cavallo, 1966).

$$e = 1.78\left(1 - 0.045AR^{0.68}\right) - 0.64 \tag{30}$$

where AR is the aspect ratio of the wing. Equation (30) can be alternatively presented as

$$e = 1.78\left(1 - 0.045\left(\frac{b}{c}\right)^{0.68}\right) - 0.64 \tag{31}$$

At any steady flight point, the parasitic drag increases linearly as the span of the wing increases. In contrast, the vortex-induced drag reduces approximately with the square of the span. The variation in total wing drag with wing span at the start of loiter and end of loiter is shown in Figure 13(a) and (b).

For the start of loiter, initially the induced drag of the wing is higher than the parasitic drag. As the wing span increases (symmetrically), the induced drag decreases while the parasitic drag increases. They become equal at 18% symmetric increase in wing span. The minimum total drag of the wing occurs at 40% increase in wing span resulting in 13% reduction in the total wing drag. It turns out that in the region between 20% and 60% increase in wing span, the total drag is almost uniform. At 20%, the total drag reduces by

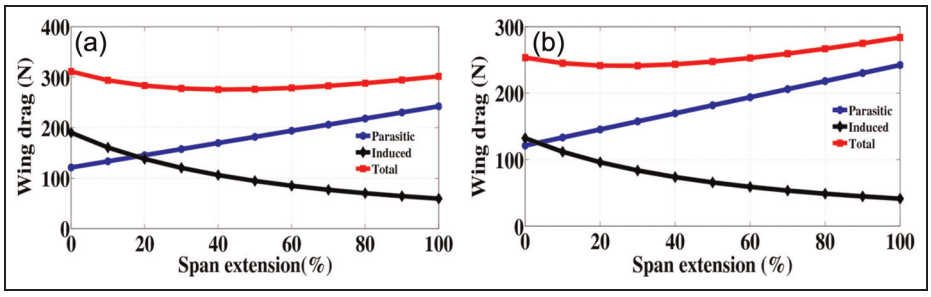

Figure 13. Variation of wing drag with symmetric span extension at BOW = 500 kg, M0.16, 20,000 ft: (a) wing drag at the start of loiter (790 kg) and (b) wing drag at the end of loiter (660 kg).
BOW: basic operating weight.

Table 9. Drag reduction from symmetric span morphing.

Flight point	Vehicular weight (kg)	Speed (m/s)	Altitude (m)	Drag reduction (%)	Optimum span extension (%)
Start of loiter	790	50	6100	13.0	43
End of loiter	660	50	6100	4.8	26

10%, while at 60% the total drag reduces by 9.5%. From a structural point of view, it is more feasible to increase the wing span by 20% to reduce the total drag by 10% rather than increasing the span by 40% to get 11% reduction in the total drag. For the end of loiter flight point, initially the parasitic drag is higher than the induced drag. This because the UAV is flying at the same altitude but now it has to generate lower lift, and hence lower induced drag. It turns out that the minimum wing drag occurs at 30% increase in wing span resulting in a 4.8% reduction in the drag. Any further increase in the span increases the drag as the increase in parasitic drag component starts to dominate the reduction in induced drag. This is summarised in Table 9.

The effectiveness of symmetric span morphing to reduce the drag depends on the drag breakdown. In other words, it depends on the relative magnitude of the parasitic drag and the vortex-induced drag. For flight points where the wing is generating a large lift, morphing the span can be very effective, but when the wing is generating little lift, excessive span extension can increase the drag rather than reduce it. Nevertheless, increasing the wing span for low lift flight phases can be effective, for example, landing where the increase in drag is required to reduce the LD. By examining equation (29), for any given flight conditions and instantaneous vehicular weight, the span that minimises the total wing drag can be obtained by taking the derivative of the total drag with respect to the wing span at constant speed (U) and altitude/density (ρ) and setting it to zero as

$$\left.\frac{\partial D}{\partial b}\right|_{U,\rho} = 0 \tag{32}$$

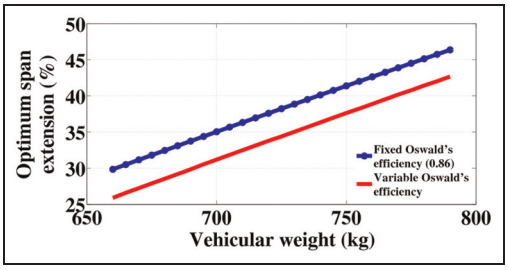

Figure 14. Variation of optimum span with vehicular weight at M0.16, 20,000 ft.

Hence, the span that produces the minimum wing drag, assuming constant e, is

$$b_{min} = \left(\frac{2(Wg)^2 g}{\pi q^2 e c C_{f_e}}\left(\frac{S}{S_{wet}}\right)\right)^{1/3} \approx \left(\frac{(Wg)^2}{\pi q^2 e c C_{f_e}}\right)^{1/3} \tag{33}$$

Equation (33) indicates that for a given flight condition, the wing span that produces the minimum drag is proportional to ($W^{2/3}$). This means that as the vehicle burns fuel and as its weight reduces the span that produces the minimum drag reduces because the effectiveness of span morphing reduces as the vehicular weight decreases.

Figure 14 shows the variation of optimum span with the instantaneous weight at a constant altitude and flight speed. The line marked with dots is the optimum span for a constant e of 0.86, whereas the other line is for a variable (variation with span). The two lines have almost the same slope. At the start of loiter where the weight is 790 kg, the optimum symmetric span

extension to minimise drag for a fixed e is 47%, extension, and for variable e, it is 43% extension. On the contrary, at the end of loiter where the weight is 660 kg, the optimum symmetric span extension for fixed e is 30% and for a variable e is 26%.

Optimal flight speed

The total drag of the UAV (induced and parasitic drag of the wing, fuselage and empennage) can be expressed as

$$D = D_i + D_o \tag{34}$$

The parasitic drag component can be approximated as

$$D_o = qc\left(C_{Do_w} b_{new} + b\left(C_{Do_f} + C_{Do_E}\right)\right) \tag{35}$$

where C_{Do_f} is the parasitic drag coefficient of the fuselage, C_{Do_E} is the parasitic drag coefficient of the empennage (normalised by the original wing reference area) and b_{new} is the wing span after morphing. It should be noted that the parasitic drag of the fuselage and empennage are constant regardless of the wing span, and hence their coefficients are multiplied by the original reference area of the wing (before morphing), since their values are extracted from Tornado VLM before morphing occurs. Tornado employs the semi-empirical component build-up method (Cavallo, 1966) to estimate the parasitic drag (including form drag) of the vehicle. The fuselage is modelled as a cylinder with equivalent diameter. Typical values of these drag coefficient are taken from Tornado VLM where $C_{Do_f} = 0.0028$ and $C_{Do_E} = 0.002$. According to equation (28), C_{Do_w} is constant, but in equation (35) it is multiplied by b_{new} because the parasitic drag of the wing varies with span morphing although C_{Do_w} remains constant. The total drag equation becomes

$$D = qc\left(C_{Do_w} b_{new} + b\left(C_{Do_f} + C_{Do_E}\right)\right) + \frac{g^2}{\pi q e}\left(\frac{W}{b}\right)^2 \tag{36}$$

By further expanding q in the above equation, one can notice that for a given vehicular weight and wing span, there exists a flight speed that can minimise the total drag of the vehicle. Using equation (32), this optimal flight speed can be expressed as

$$U_{min} = \left(\frac{4g^2}{\pi e c \rho^2 \left(C_{Do_w} b_{new} + b\left(C_{Do_f} + C_{Do_E}\right)\right)}\left(\frac{W}{b_{new}}\right)^2\right)^{0.25} \tag{37}$$

The variation of optimal speed with span extension for different vehicular weights is shown in Figure 15.

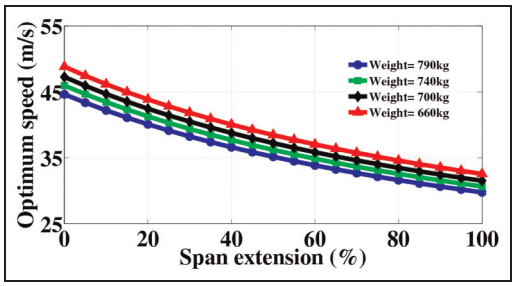

Figure 15. Variation of optimum flight speed with span extension at M0.16, 20,000 ft.

As the instantaneous vehicular weight reduces (with burning fuel), the optimal speed for a given span extension increases. For instance, at 10% span extension, the optimal speed increases from 42 m/s at 790 kg to 46 m/s at 660 kg. On the contrary, for a given instantaneous vehicular weight, increasing the wing span reduces the optimal flight speed. For instance at a vehicular weight of 790 kg, the optimal speed decreases from 49 m/s at 0% span extension to 32 m/s at 100% span extension.

Endurance and sensitivity to weight

The baseline configuration of the UAV has an endurance of about 18 h. The objective of this section is to estimate the increase in endurance that can be achieved with symmetric span morphing. The rate of change of vehicular weight can be expressed as (Filippone, 2006)

$$\frac{dW}{dt} = -TC = -DC \tag{38}$$

where T is thrust and at a steady level flight it is equal to total drag (D), and C is the specific fuel consumption for a given throttle setting. The specific fuel consumption (C) in h^{-1} can be expressed as

$$C = \frac{C_{bhp}(3.3U)}{550\eta_p} \tag{39}$$

where C_{bhp} is the propeller-specific fuel consumption and η_p is the propeller efficiency factor. The UAV considered here has a Rotax 914 piston engine with a propeller-specific fuel consumption of 0.458 lb/h/bhp (Rotax Aircraft Engines, 1998) and a propeller efficiency factor of 0.70 (for fixed pitch angle) (Raymer, 2006). The endurance of the vehicle becomes

$$E = \int_{t_1}^{t_2} dt = -\int_1^2 \frac{dW}{CD} \tag{40}$$

The baseline UAV has an estimated basic operating weight (BOW) of 500 kg. The incorporation of the span morphing technology on board the UAV can increase the BOW mainly due to the actuator and the structural layout to support morphing and the need for a stiffer

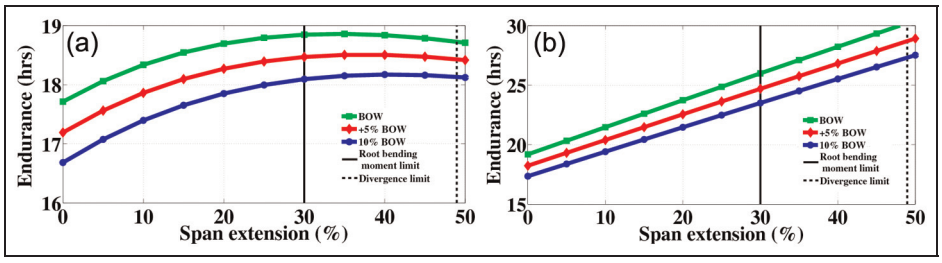

Figure 16. Variation of endurance with symmetric span extension for different BOWs: (a) variation of endurance with span extension for different BOWs at 50 m/s, 20,00 ft and (b) variation of endurance with span extension for different BOWs at optimal speed, 20,000 ft.
BOW: basic operating weight.

and stronger structure to support the higher aerodynamic loads. This can limit or reduce the benefits of symmetric span extension in reducing vortex-induced drag and increasing the endurance of the vehicle. To determine the sensitivity of endurance to the operating weight, two cases were considered. The first case is when the BOW increases by 5% (equivalent to 20% increase in wing weight) and the second case is when the BOW increases by 10% (equivalent to 40% increase in wing weight). For both cases the amount of fuel available is similar to that of the baseline and equal to 150 kg. For each BOW, the endurance of the UAV is evaluated for different span extension at a fixed flight speed of 50 m/s at 20,000 ft and at the optimal flight speed (associated with different wing spans and different BOWs). As the wing span increases, the bending moment at the root increases. A limit on the root bending moment is set where the bending moment at the root produced by span extension must not exceed that produced by 10° aileron deflection by more than 25%. This corresponds to a span extension of 30%. On the contrary, the increase in wing span affects the aeroelastic behaviour of the wing reducing its divergence and flutter speed. Static divergence is considered in this analysis and flutter shall be considered in future work. According to Fung (2002), for a cantilever rectangular wing with uniform structural and geometric properties along its span, the span at which divergence is initiated can be approximated as

$$b_{div} = \frac{1}{U_{crit}}\sqrt{\frac{\pi^2 GJ}{2\rho x_{sc} c C_{L_\alpha}}} \tag{41}$$

Table 10. Wing design parameters (Ajaj et al., 2012a).

Design parameter	Value
Torsional rigidity (GJ)	0.81×10^6 Nm^2
Lift moment arm (x_{sc})	0.374 m
Lift curve slope (C_{L_α})	4.875 rad^{-1}
Critical speed (U_{crit})	75 m/s

where GJ is the torsional rigidity of the wing, x_{sc} is the distance between aerodynamic centre and shear centre and U_{crit} is the critical flight speed which can be approximated as 120% of the design dive speed of the vehicle according to FAR 23 Regulations (23.629 Flutter). Ajaj et al. (2012a) have conducted aeroelastic studies on the wing of this MALE UAV and they have estimated the properties of the wing assuming a two-spar wingbox made of Aluminium 2024-T3. The design parameters of the wing as taken from Ajaj et al. (2012a) are listed in Table 10.

Figure 16(a) shows the variation of endurance with span extension at a fixed flight speed for the three BOWs (baseline, + 5% and + 10%). It can be seen that the endurance increases with span extension up to a certain point where any further increase in span results in reduction in the endurance. As the BOW increases, the ability to increase the baseline endurance capability (18 h) reduces and the point of maximum endurance shifts to the right. This is summarised in Table 11.

From Table 11, one can notice that as the BOW increases, the span extension at which maximum endurance occurs shifts from 34% for the baseline to 40%

Table 11. Gain in endurance due to symmetric span morphing at fixed speed.

Case	Initial endurance (h)	Endurance at root bending limit (h)	Endurance at 22% extension (h)	Gain in endurance (%)	Gain in endurance with respect to baseline (%)
Baseline	17.71	18.85	18.73	6.5	6.5
+ 5% BOW	17.19	18.50	18.32	7.7	4.5
+ 10% BOW	16.68	18.10	17.90	8.9	2.6

BOW: basic operating weight.

Table 12. Gain in endurance due to symmetric span morphing at optimum speed.

Case	Initial endurance (h)	Endurance at root bending limit (h)	Endurance at 22% extension (h)	Gain in endurance (%)	Gain in endurance with respect to baseline (%)
Baseline	17.71	26.00	24.20	36.6	36.6
+ 5% BOW	17.19	24.70	23.00	33.8	29.8
+ 10% BOW	16.68	23.50	21.90	31.3	23.6

BOW: basic operating weight.

when the BOW increases by 10%. As was shown in section 'Roll rate', the optimum span morphing for roll control is 22% extension of one side of the wing and 22% retraction of the other side. The endurance at 22% symmetric span extension is 18.73 h for the normal BOW. This corresponds to 0.7% reduction in the maximum allowed endurance (at the root bending moment limit) that can be achieved by symmetric span morphing.

On the contrary, the variation of endurance with span extension at optimum flight speed is almost linear for different BOWs. Figure 16(b) shows the significant increase in endurance that can be achieved with span morphing (symmetric extension) at the optimal flight speed. The results are summarised in Table 12. The gain in endurance due to span morphing relative to the baseline configuration is significant up to 36.6%.

There are two main contributors other than span extension to this large increase in endurance. The first one is the minimal total drag that can be achieved when flying at optimal speed, while the second one is the reduction in fuel consumption achieved with reducing the flight speed (equation (41)). For a fixed flight speed, the increase in wing span results in an increase in the endurance up to a certain limit where any further increase in span reduces the endurance (as increase in parasitic drag dominates the decrease in vortex-induced drag). On the contrary, for an optimal flight speed, the increase in wing span results in a continuous increase in endurance (almost linear variation). However, from an operational and control point of view, there are lower limits in terms of the feasibility of reducing flight speed to minimise drag. These limits depend on the stall speed, minimum control speed, mission objectives and various other design requirements. Possibly, up to 10% reduction in flight speed can be tolerated given the large increase in endurance.

Static stability

The UAV has a V-tail empennage configuration and it has a horizontal tail volume coefficient (c_{HT}) of 0.73 and a vertical tail volume coefficient (c_{VT}) of 0.057. The tail coefficients can be expressed as (Raymer, 2006)

$$c_{VT} = \frac{x_{VT} S_{VT}}{bS} \tag{42}$$

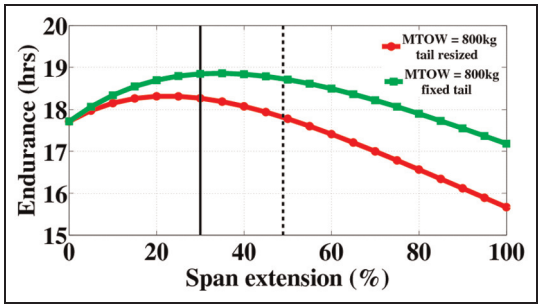

Figure 17. Endurance versus span extension for different empennage configurations.
MTOW: maximum take-off weight.

and

$$c_{HT} = \frac{x_{HT} S_{HT}}{\bar{c}S} \tag{43}$$

where x_{VT} and x_{HT} are the moment arms of the vertical and horizontal tail, respectively, S_{VT} and S_{HT} are the projected area of the vertical tail (on the vertical plane) and horizontal tail (on the horizontal plane), respectively. Equations (44) and (45) show that as the wing span increases, the HT and VT volume coefficients reduce, and hence their effectiveness. In order to keep constant volume coefficient the tail must be resized accordingly as the wing span increases. This increases the drag contribution of both the HT and VT, and hence reduces the endurance benefits that can be achieved with symmetric span morphing as shown in Figure 17.

Figure 17 shows that if the tail is sized with each wing span (neglecting the change of the tail weight), the benefits in endurance that can be achieved with span morphing reduce significantly in comparison with the previous case where the tail size is fixed. The maximum endurance is 18.3 h and occurs at 20% span extension, while for the fixed tail case the maximum endurance is 18.86 h and occurs at 34% span extension. The maximum endurance reduces by about 3%.

It should be noted that the position of the neutral point is almost fixed because the lift generated by the wing is constant and equals the instantaneous vehicular weight, so as the wing span increases, the lift coefficient (AOA) is reduced to maintain level flight. Furthermore, the symmetric morphing of the wing will not affect the

position of the centre of gravity of the vehicle as the wing has zero sweep angle. This means that the static margin of the UAV is constant and independent of the wing span.

From an operational point of view, extending the span symmetrically reduces the tail effectiveness, for instance in spin recovery, however, if such an extreme flight condition arises when the wing span is fully morphed, it is sufficient to revert to the baseline configuration for which the tail has its maximum effectiveness.

Take-off and landing

The UAV studied here does not have a flap to increase the lift coefficient at take-off and landing. The span morphing technology incorporated for roll control and drag reduction can be used during the low-speed transitional phases to increase the lift coefficient and the wing area to reduce the take-off field length (TOFL) and LD. From the above section each semi-span of the wing must be capable of 22% extension and 22% retraction. Raymer (2006) provides a semi-empirical correlation to approximate the TOFL and LD. According to Raymer (2006), the TOFL (m) can be approximated as

$$\text{TOFL} = A(TOP) + B \tag{44}$$

where A and B are constants and can be approximated as 1100 and -55, respectively, while TOP is the take-off parameters and for a propeller-driven vehicle is given as

$$TOP = \frac{(W_{To}/S)}{\sigma C_{L_{TO}}(P/W)} \tag{45}$$

where (W_{To}/S) is the wing loading at take-off in kg/m^2, (P/W) is the power to weight ratio in W/kg, $C_{L_{TO}}$ is the take-off lift coefficient and σ is the density ratio and is assumed to be unity in this analysis. On the contrary, the LD (m) can be approximated as (Raymer, 2006)

$$LD = 5\left(\frac{W_{LD}/S}{\sigma C_{L_{max}}}\right) + S_a \tag{46}$$

where (W_{LD}/S) the wing loading during landing, $C_{L_{max}}$ is the maximum lift coefficient and S_a is a constant and can be approximated as 183 m for this UAV. The initial maximum lift coefficient for this UAV is approximated to be 1.20, and the lift coefficient during take-off is about 0.992. The engine (Rotax 914) has a rated power of 100 hp (74.5 kW) at take-off (Rotax Aircraft Engines, 1998). For a given vehicular weight and engine, the fractional change in $C_{L_{max}}$ due to span extension can be approximated using the fractional change theory developed by Isikveren (2002, 2003) as

$$\Delta C_{L_{max}} = \frac{(1 + \Delta AR)}{3 + \xi}\left\{\xi(1 + \Delta AR)^{\phi-1} + 3\right\} - 1 \tag{47}$$

and

$$\xi = \frac{C_{L_{max_0}}}{k_{geo} AR_0} \tag{48}$$

where ΔAR is the fractional change in aspect ratio due to span morphing, AR_0 is the aspect ratio before morphing, $C_{L_{max_0}}$ is the maximum lift coefficient before morphing and k_{geo} and ϕ are geometric constants given as 0.002183 and 0.475, respectively, in Isikveren (2002). For the above equations to be valid, the quarter chord sweep must be zero and there must be no change in sweep, also there must be no change in the thickness to chord ratio, and there must be no flap. For this analysis, equation is valid since all the aforementioned conditions are not violated. The maximum lift coefficient after morphing is given as

$$C_{L_{max}} = C_{L_{max_0}}(1 + \Delta C_{L_{max}}) \tag{49}$$

According to Raymer (2006), $C_{L_{TO}}$ after morphing can be estimated as

$$C_{L_{TO}} = \frac{C_{L_{max}}}{1.21} \tag{50}$$

The variations of TOFL and LD (for normal landing at the end of loiter) with span extension at different BOWs are shown in Figure 18(a) and (b), respectively. Both the TOFL and LD (for normal landing at the end

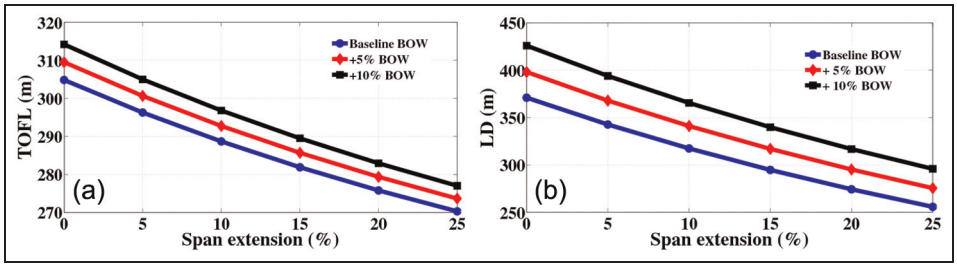

Figure 18. Benefits of symmetric span extension during take-off and landing: (a) take-off and landing distances and (b) increase in allowable take-off and landing weights.
TOFL: take-off field length; BOW: basic operating weight.

Table 13. Reduction in TOFL and LD due to span morphing.

Weight scenarios	TOFL at 0% span extension (m)	TOFL at 22% span extension (m)	LD at 0% span extension (m)	LD at 22% span extension (m)
Baseline BOW	305	274	371	267
+ 5% BOW	310	277	398	287
+ 10% BOW	314	281	426	308

TOFL: take-off field length; LD: landing distance; BOW: basic operating weight.

Table 14. Actuation forces and powers required for span morphing.

Actuation time (s)	Acceleration (m/s^2)	Maximum speed (m/s)	Force (N)	Power (W)
0.5	10.6	5.40	139	736
1.0	2.60	2.60	35.0	92.0

of loiter) decrease significantly with span extension. It should be noted that in this section the power delivered by the engine is fixed, that is, the same engine is still in use. Table 13 summarises the outcomes of the analysis.

Table 13 shows that a 10% reduction in TOFL and a 28% reduction in LD can be achieved at 22% span extension for all the weight scenarios. Since span morphing allows the TOFL and LD to be controlled, the UAV can operate with a range of payloads without exceeding operational performance constraints which increases the vehicle operational efficiency.

Actuator sizing

In order to have an initial estimate of the actuator size required (force, power and volume), a telescopic (sliding) span morphing mechanism is considered. In the sizing process, frictional losses due to the sliding mechanism and other forms of losses are ignored and only inertial forces are considered. Frictional losses are ignored mainly because detailed knowledge about the mechanism is not available and the aim of this study is to perform preliminary investigation of the benefits and actuation requirements of the span morphing technology. The morphing span moves perpendicular to the airflow (due to sweep being zero), and hence the aerodynamic resistance is negligible. The actuator is sized for a 22% extension or retraction which is the largest displacement to be considered. To estimate the power, uniform acceleration actuation is considered. This means that the maximum actuation power can be expressed as

$$P_{max} = FV_{max} \tag{51}$$

where

$$F = m_p a \tag{52}$$

and

$$V_{max} = at_{max} \tag{53}$$

and a is the acceleration, m_p is the mass of the morphing partition and is estimated to be 13 kg, and t is the total actuation time. The maximum displacement of the morphing partition is $x = 1.32$ m (22% of the semi-span). For uniform accelerated actuation, the displacement for full extension can be expressed as

$$x = \frac{1}{2} a t_{max}^2 = 1.32\,\text{m} \tag{54}$$

Rearranging equation (51), the maximum actuation power required is

$$P_{max} = 1.625 m_p a^{3/2} \tag{55}$$

Table 14 shows the actuation force and power required for different actuation times. To move the morphing partition (on one side of the wing) in 1 s, an actuation force of 35 N and an actuation power of 92 W are required.

The total structural weight of the ailerons and their support is estimated to be 15 kg using semi-empirical equations from Torenbeek (1992). The chord of the aileron is 0.375 m (20% of the local chord). The mass moment of inertia per aileron is 0.35 kg m^2. Unlike span morphing, the aerodynamic resistance on the aileron can be higher than its inertia as it opposes the airflow while it is deflecting. The hinge moment at the maximum aileron deflection is estimated to be 37 Nm per aileron (Abbott and Von Doenhoff, 1959). Table 15 shows the actuation force and power required for the aileron (on one side of the wing) at different actuation times.

To move the aileron in 1 s, an actuation moment of 37 N and an actuation power of 13 W are required. The power required to move the aileron in 1 s is about 14% of the power needed to move the morphing span in 1 s.

Electromechanical actuators are the most promising actuation system for this application due to their

Table 15. Actuation forces and powers required for aileron.

Actuation time (s)	Angular acceleration (rad/s^2)	Maximum angular speed (rad/s)	Moment (Nm)	Power (W)
0.5	1.40	0.70	37.5	26.0
1	0.35	0.35	37.0	13.0

simplicity and ease of integration in comparison to hydraulics, pneumatics or other exotic actuators. Electromechanical actuators have a specific work of about 300 J/kg (Ajaj et al., 2012b). Moving the wing span in 0.5 s is associated with actuation energy of 184 J. This corresponds to an actuator weight of 0.613 kg on each side of the wing. On the contrary, moving the aileron in 0.5 s is associated with actuation energy of about 7 J which corresponds to an actuator weight of 0.022 kg on each side of the wing. The ratio of actuator weight associated with span morphing to that associated with ailerons is about 28.

Operating the morphing technology

The span morphing technology provides control authority and operational performance benefits. When operating this technology during flight, stability and control are always given the priority over operational performance. This is because stability and control are of primary concern for the safety and survivability of the vehicle. Usually roll control lasts for a short period of time, so even if the wing span is not optimum to maximise endurance during this period of time for control, it will have very limited impact on the gain in endurance provided by the span morphing technology. In some flight scenarios, it is possible to have sufficient rolling authority with a large overall wing span (optimum for performance), but since this is not always feasible (depending on the roll rate demanded) stability and control are always given the priority.

Conclusion

The morphing span technology is effective for replacing conventional ailerons and for enhancing the flight performance of a MALE UAV. The largest increases in wing semi-span required to meet the rolling moment requirement occur at the end of loiter phase, that is, prior to descent.

Unlike ailerons, the rolling moment generated by span extension is very sensitive to the instantaneous vehicular weight and the AOA. This proves that morphing structures should not be operated in the same way as conventional control surfaces. The benefits that can be achieved from coupled manoeuvres must be exploited via the design of 'ad hoc' flight control systems. The optimum rolling strategy from control, structural and aerodynamic points of view is to extend the semi-span of one side of the wing by 22% and to retract the other by 22%.

Span morphing induces some additional inertial terms in the roll equation of motion. Furthermore, the importance of the transient response increases with span morphing when compared to ailerons due to the larger and heavier structure that must be actuated.

In terms of flight performance, a 34% symmetric span extension was found to be optimum from an aerodynamic point of view, resulting in a 6.5% increase of the baseline endurance. However, in the region from 20% to 50% symmetric span extension, the change in endurance is minimal. Therefore, structural limitations dictate the optimal choice for the span extension magnitude. Considering such limitations, in order to maximise the roll authority and flight endurance, each side of the wing must be designed to extend by 22% and to retract by 22%. Finally, the wing designed to extend and retract up to 22% can achieve a 28% reduction in TOFL and a 10% reduction in LD. In this study, morphing technology was added to an existing air vehicle which required modifying the geometry and the structure of the vehicle to fit the technology. However, this approach of retro-fitting constrained the benefits of morphing due to the higher weight and complexity of the technology. Therefore, in order to exploit the benefits of morphing, it has to be considered early in the design process. In other words, morphing aircraft are superior to aircraft with morphing.

Acknowledgements

R.M.A. acknowledges support and feedback from the Visionary Aircraft Concept (VAC) Group at Bauhaus Luftfahrt e.V., Munich, Germany. E.I.SF acknowledges the support from the Department of Civil Engineering, University of Santiago, Chile, and also from the National Commission for Scientific and Technological Research (CONICYT), from the Chilean government.

Declaration of conflicting interests

The authors declared no potential conflicts of interest with respect to the research, authorship, and/or publication of this article.

Funding

This work was supported by the European Research Council through grant number 247045 entitled *Optimisation of Multiscale Structures with Applications to Morphing Aircraft*.

References

Abbott IH and Von Doenhoff AE (1959) *Theory of Wing Sections: Including a Summary of Airfoil Data*. New York: Dover Publications Inc.

Ajaj RM, Friswell MI, Dettmer WG, et al. (2012) Dynamic modelling and actuation of the adaptive torsion wing. *Journal of Intelligent Material Systems and Structures*. Epub ahead of print 17 July. DOI: 10.1177/1045389X12444493.

Ajaj RM, Friswell MI, Saavedra-Flores EI, et al. (2012a) Span morphing: a conceptual design study. In: *20th AIAA/ASME/AHS adaptive structures conference*, Honolulu, HI, 23–26 April, paper no. American Institute of Aeronautics and Astronautics (AIAA). 2012-1510.

Ajaj RM, Saavedra-Flores EI, Friswell MI, et al. (2012b) The Zigzag wingbox for a span morphing wing. *Aerospace Science and Technology*, 28(1): 364–375.

Anderson JD (1991) *Fundamentals of Aerodynamics*. 2nd ed. McGraw-Hill, New York, USA.

Austin R (2010) *Unmanned Aircraft Systems: UAV Design, Development, and Deployment*. John Wiley & Sons Ltd, Sussex, UK. 313 pp.

Barbarino S, Bilgen O, Ajaj RM, et al. (2011) A review of morphing aircraft. *Journal of Intelligent Material Systems and Structures* 22(9): 823–877.

Blondeau J and Pines D (2007) Design and testing of a pneumatic telescopic wing for unmanned aerial vehicles. *Journal of Aircraft* 44(4): 1088–1099.

Blondeau J, Richeson J and Pines DJ (2003) Design, development and testing of a morphing aspect ratio wing using an inflatable telescopic spar. In: *44th AIAA/ASME/ASCE/AHS/ASC structures, structural dynamics and materials conference*, 7–10 April 2003, Norfolk, VA, paper no. AIAA 2003-1718.

Bye DR and McClure PD (2007) Design of a morphing vehicle. In: *48th AIAA/ASME/ASCE/AHS/ASC structures, structural dynamics, and materials conference*, Honolulu, HI, 23–26 April 2007, paper no. American Institute of Aeronautics and Astronautics (AIAA) 2007-1728.

Cavallo B (1966) *Subsonic drag estimation methods*. Report no. NADC-AW-6604, US Naval Air Development Centre.

Chipperfield AJ and Fleming PJ (1995) The MATLAB genetic algorithm toolbox. *In: Proceedings of the IEE colloquium on applied control techniques using MATLAB, Digest no. 1995/014,* Institution of Electrical Engineers, London, UK.

Filippone A (2006) *Flight Performance of Fixed and Rotary Wing Aircraft*. 1st Edition, Butterworth-Heinemann, Oxford, UK.

Fung YC (2002) *An Introduction to the Theory of Aeroelasticity*. New York: Dover Publications Inc.

Isikveren AT (2002) *Quasi-analytical modelling and optimisation techniques for transport aircraft design*. Doctoral Thesis, Royal Institute of Technology (KTH), Sweden. Report 2002-13.

Isikveren AT (2003) Parametric modeling techniques in industrial conceptual transport aircraft design. SAE technical paper 2003-01-3052, 2003. DOI: 10.4271/2003-01-3052.

Ivanco TG, Scott RC, Love MH, et al. (2007) Validation of the Lockheed Martin morphing concept with wind tunnel testing. *In: 48th AIAA/ASME/ASCE/AHS/ASC structures, structural dynamics, and materials conference*, American Institute of Aeronautics and Astronautics, 23-26 April 2007, Honolulu, HI, paper no. AIAA 2007-2235.

Love MH, Zink PS, Stroud RL, et al. (2007) Demonstration of morphing technology through ground and wind tunnel tests. In: *48th AIAA/ASME/ASCE/AHS/ASC structures, structural dynamics, and materials conference*, American Institute of Aeronautics and Astronautics, 23–26 April 2007, Honolulu, HI, paper no. AIAA 2007-1729.

McCormik BW (1995) *Aerodynamics, Aeronautics and Flight Mechanics*. 2nd ed. New York: Wiley.

Melin T (2000) *A vortex lattice MATLAB implementation for linear aerodynamic wing applications*. Master's Thesis, Department of Aeronautics, Royal Institute of Technology (KTH), Sweden.

Nelson RC (1989) *Flight Stability and Automatic Control*. 1st ed. McGraw-Hill, New York, USA.

Raymer DP (2006) *Aircraft Design: A Conceptual Approach*. 4th ed. American Institute for Aeronautics and Astronautics (AIAA), Virginia, USA.

Roskam J (2003) *Airplane Design, Part V: Component Weight Estimation*. Lawrence, KS: DARcorporation.

Rotax Aircraft Engines (1998) *Operator's Manual for All Versions of Rotax 914*. BRP-Powertrain GmbH & Co KG, Austria.

Seigler TM, Bae JS and Inman DJ (2004) Flight control of a variable span cruise missile. In: *Proceedings of 2004 ASME international mechanical engineering congress and exposition*, Anaheim, CA, 13–19 November, American Society of Mechanical Engineers (ASME), paper no. IMECE2004-61961.

Torenbeek E (1992) *Development and application of a comprehensive, design-sensitive weight prediction model for wing structures of transport category aircraft*. Report no. LR-693, September. Delft University of Technology.

Weisshaar TA (2006) *Morphing aircraft technology – new shapes for aircraft design*. Report no. RTO-MP-AVT-141. 01 October 2006, France: Neuilly-sur-Seine.

Appendix 1

Notation

AR	aspect ratio
b	span
c	wing chord
$\bar{c}$	mean aerodynamic chord
C	specific fuel consumption
C_D	drag coefficient
C_{f_e}	equivalent skin friction coefficient
C_l	rolling moment coefficient
C_L	lift coefficient
C_{l_p}	rolling moment damping coefficient
C_{L_α}	lift curve slope
C_n	yawing moment coefficient
D	drag
e	Oswald's efficiency
E	endurance
g	gravitational acceleration
GJ	torsional rigidity

I_{xx}	mass moment of inertia about the x-axis
L	lift
L	rolling moment
m	mass
p	roll rate
P	power
q	dynamic pressure
S	reference area
S_a	landing distance constant
T	thrust
U	airspeed
W	vehicular weight
x	moment arm
y	increment in wing semi-span
δ	aileron angle
η_p	propeller efficiency
ρ	air density
σ	density ratio
τ	time constant

Subscripts

a	ailerons
$crit$	critical
div	divergence
E	empennage
f	fuselage
HT	horizontal tail
i	induced drag
LD	landing
max	maximum
new	new (after morphing)
o	parasitic drag
p	morphing partition
s	span morphing
sc	shear centre
TO	take-off
VT	vertical tail
w	wing
wet	wetted area
0	initial (before morphing)
1	starboard wing
2	port wing